Title
Grinding energy modeling based on friction, plowing and shearing

Authors
Linke, Barbara
Garretson, Ian
Torner, Francois M
et al.

Publication Date
2017-07-12

DOI
10.1115/1.4037239

Peer reviewed

Journal of Manufacturing Science and Engineering. Received March 30, 2017;
Accepted manuscript posted July 13, 2017. doi:10.1115/1.4037239

Grinding energy modeling based on friction, plowing and shearing

Barbara S. Linke
University of California Davis, Mechanical and Aerospace Engineering Department
1 Shields Ave, Davis, CA 95616
USA
bslinke@ucdavis.edu
ASME member

Ian Garretson
University of California Davis, Mechanical and Aerospace Engineering Department
1 Shields Ave, Davis, CA 95616
USA
icgarretson@ucdavis.edu

Francois Torner
University of Kaiserslautern
Institute for Measurement and Sensor-Technology
Gottlieb-Daimler-Straße
67663 Kaiserslautern
Germany
torner@mv.uni-kl.de

Joerg Seewig
University of Kaiserslautern
Institute for Measurement and Sensor-Technology
Gottlieb-Daimler-Straße
67663 Kaiserslautern
Germany
seewig@mv.uni-kl.de

ABSTRACT

Grinding is an important abrasive machining process at the end of many process chains. Understanding energy transformation in grinding is not only important to improve energy efficiency, but it is crucial for understanding the chip formation process itself. Grinding energy can be studied at the macroscopic or microscopic levels, wherein the entire grinding tool is considered or the phenomena at the single cutting edges are studied. This paper explores existing energy modeling approaches in grinding with particular emphasis on physical models. Models on energy transformation during the ductile grit-workpiece engagement for three regimes — being friction, plowing, and shearing — are explained. In addition to the critical depth of cut when chip formation starts, a critical depth when plowing begins is introduced to divide between the different regimes. Selected models for each regime are combined to an integrated grinding energy model that allows researchers to investigate forces and energy during grit engagement.

INTRODUCTION

The industrial sector is responsible for a substantial part of today`s energy consumption [1]. In 2011, 24.0 quadrillion Btu were consumed in the industrial sector, which is approximately one-third of total U.S. delivered energy [2]. In addition, sustainability in manufacturing is a driving force for companies as producers are becoming more responsible for their products [1, 3].

Grinding is a high performance abrasive technology with high process stability and quality [4, 5]. Grinding is either applied to improve part quality (e.g. automotive components, functional surfaces, optical devices, dies and molds) or to shape difficult-to-cut materials (e.g.

turbine blades, cutting tools, lead screws). Grinding procedures are typically applied towards the end of production chains and define part surface topography and integrity.

An energy study performed at MIT in 2005 estimated that 63 petajoules are consumed by grinding per year in the US alone [6]. However, according to a CIRP Round Robin test, the specific energy required for the grinding process itself amounts only to 10 to 20 percent of the energy of the entire grinding machine system [7]. The comprehensive energy consumption and equivalent carbon dioxide emission during the grinding process should consider direct energy consumption, resource utilization, waste generation and their collective effect on equivalent carbon dioxide emission [8].

Although research on the physical phenomena in grinding is well established, there is no generic physical model on energy consumption of grinding. Grinding tools are inherently stochastic, because the abrasive grits are of irregular geometry and the grits change over time, due to wear, all of which makes modeling a challenging endeavor [9, 10]. This paper explores existing modeling approaches for energy in grinding with particular emphasis on physical models. Grinding energy will be discussed at both macroscopic and microscopic perspectives, which consider either the entire grinding tool or a single cutting edge respectively. An integrated energy model is proposed and demonstrated with a case study to grind steel. In the future, the model can be adapted to case-specific research findings and include the stochastic nature of the abrasive grits.

ENERGY CONVERSION IN GRINDING

In grinding, abrasive grits engage with the workpiece to form chips. A bonding agent is utilized to hold the grits in place on the tool. The bonding agent also relieves grits that have become blunt them to reveal new sharp grits. Additionally, dull grits splinter and self-sharpen. Pores provide space to supply cooling lubricant and remove chips from the contact zone. Proper abrasive grit and bond design improves tool performance and tool life by controlling all the bond strength, grit relief, grit sharpening, and porosity. Metal working fluids are important to cool, reduce friction, clean, transport chips, and protect against corrosion [4, 5]. Grinding oil, water-based emulsions or watery solutions are common cooling lubricants. In addition to the media type, flow volume, flow rate, and supply systems affect the grinding process performance [4].

Knowledge of the chip formation mechanisms helps to optimize the grinding process. Material removal in grinding ductile materials involves elastic and plastic deformation, friction, and material shearing, leading to chip formation [4, 11, 12]. Material removal in brittle materials is mainly caused by crack formation and propagation, which causes the material to break away as particles. Mladenovic et al. [13] studied cutting mechanism in oxide ceramics with diamond scratch tests and found two distinct regions within the scratches: a region from the diamond grain entering the material followed by a region of chipping. Brittle materials can be machined in a ductile mode if the chip thickness is small enough [14]. Energy monitoring is helpful to detect the mode transition [14]. Unfortunately, the grinding contact zone cannot be directly observed because it is not easily accessible and contact times are very short. The

maximum undeformed chip thickness is a powerful and simple metric that explains how the main process parameters affect grinding phenomena. It can be calculated using equation 1 [12, 15-17].

Maximum undeformed chip thickness: $h_{cu,max} = \left[\frac{4}{C_{stat} r}\left(\frac{v_w}{v_{gr}}\right)\left(\frac{a_e}{d_{eq}}\right)^{1/2}\right]^{1/2}$ (1)

With C_{stat} is static cutting edge density per area; r is the proportionality factor between chip width and thickness, v_w is the workpiece speed, v_{gr} is the grinding wheel speed, d_{eq} is the equivalent grinding wheel diameter, and a_e is depth of cut

The equivalent grinding wheel diameter, d_{eq}, is used to convert the process kinematics to a surface grinding process (equations 2 - 4) with the grinding wheel diameter, d_{gr}, and workpiece diameter, d_w.

for external cylindrical grinding: $d_{eq} = \frac{d_{gr} \cdot d_w}{d_{gr} + d_w}$ (2)

for internal cylindrical grinding: $d_{eq} = \frac{d_{gr} \cdot d_w}{d_w - d_{gr}}$ (3)

for surface grinding: $d_{eq} = d_{gr}$ (4)

The static chip length (equation 5) can be calculated from the engagement between grinding wheel and workpiece [17]. The kinematic chip length takes into account that up- or down-grinding will either shorten or lengthen the contact length between wheel and workpiece (equation 6), depending on the speed ratio (equation 7).

Static chip length: $l_g = \sqrt{a_e \cdot d_{eq}}$ (5)

Kinematic chip length: $$l_k = l_g \cdot \left|1 - \frac{1}{q}\right| = \sqrt{a_e \cdot d_{eq}} \cdot \left|1 - \frac{1}{q}\right| \quad (6)$$

Speed ratio: $$q = \pm \frac{v_{gr}}{v_w} \quad (7)$$

Nearly all of the mechanical energy in the grinding process is transformed into heat [11]. The total heat flux, q_t, is a sum of the heat transferred to the chip, coolant, grinding wheel, and workpiece [18, 19]. Depending on the process conditions, the grit and wheel bonding type, 60 – 90 % of the processing energy might flow as heat into the workpiece [4]. Since this heat energy can negatively affect workpiece material and performance, it is necessary to predict and control the heat and its partition ratio, but this research will not be presented here. Grinding forces and energy consumption can be modeled from either the macroscopic or microscopic perspectives. These are respectively, the energy used during the operation of the entire spindle or the energy used during the cutting action of a single grit.

Grinding energy – macroscopic perspective

The total energy consumed to generate part shape and surface by grinding consists of processing energy, energy consumed by machine tool, and periphery and background energy (equation 8) [20]. Machine tool energy and peripheral energy can account for a significant proportion of the total energy [21]; and includes energy to run machine control, hydraulics, lighting, coolant system, compressed air, etc. Processing energy (commonly assumed to be equal to spindle energy) accounts only for 10 - 20 % of the total energy used by grinding machines [7]. On the machine level, it is acknowledged that machining processes with

geometrically defined cutting edges such as milling, drilling, or cutting, can achieve higher material removal rates with lower specific energy, i.e. processing energy divided by volume removed [22].

Grinding energy = Processing energy + machine energy + background energy (8)

In theory, the cutting power, P_c, is derived from the cutting forces in tangential, normal, and axial direction and the respective speeds (equation 9) [11]. Since the wheel speed is commonly much higher than the other speeds, the simplified equation 10 is commonly used. Most researchers work with either measured forces or measured power (equation 11) to investigate grinding processes. When measuring spindle power, the idle power has to be subtracted from the total power to get the processing power (equation 11). In addition to grinding process parameters, dressing conditions and tool wear affect the grinding power significantly [23].

Processing power from forces $P_c = F_t \cdot (v_{gr} \pm v_w) + F_n \cdot v_{fr} + F_a \cdot v_{fa}$ (9)

Processing power (simplified) $P_c = F_t \cdot v_c$ (10)

Processing power $P_c = (P_{Spindle\_total} - P_{Spindle\_idle})$ (11)

Where F_t is tangential grinding force; v_{gr} is grinding wheel speed; v_w is workpiece speed; F_n is normal grinding force; v_{fr} is radial feed rate; F_a is axial grinding force; v_{fa} is axial feed rate, v_c is cutting speed, $P_{Spindle\_total}$ is total spindle power, and $P_{Spindle\_idle}$ is spindle idle power.

Specific grinding energy, e_c, is defined as energy to remove one volumetric unit of material in [J/mm^3] [17, 24]. In the case of measured spindle power, the specific grinding

energy is calculated from the integral of processing power P_c varying over time t and material removal rate Q_w (equation 12).

Specific processing energy from measured power: $$e_c = \frac{\int P_c(t)dt}{Q_w} \quad (12)$$

A higher material removal rate decreases specific processing energy for the same volume of material removed [5, 25]. This results from the decreasing processing time, which dominates over the increasing processing power demand. Nevertheless, higher material removal rates causes higher process forces, larger tool wear, and higher surface roughness. A recent CIRP Round Robin test confirms that little information on energy use in abrasive machining is available and is hard to comparable because of a high number of process variables [7]. This reinforces the need for research on energy use in grinding processes.

Hahn [26] defined two regimes of grinding, distinct by the dominant forces and result in different energy consumption. In the first regime, cutting energy dominates and normal grinding force is linear to feed rate. And in the second, rubbing and plowing energy dominate and normal force increases disproportionately with feed rate. Typically the second regime occurs for difficult-to-machine materials.

Grinding energy – microscopic perspective

The specific energy for cutting, grinding, and polishing processes is inversely related to the average chip thickness [17, 27]. The specific grinding energy, e_c, is a sum of the energy for forming of grinding chips, e_{ch}, energy for deforming and plowing material, e_{def}, energy for sliding and overcoming friction between grinding grits, tool bond, and workpiece, e_{fr}, and the

kinetic energy of the chips, e_{kin} (equation 13) [11, 17]. The kinetic chip energy is usually assumed to be negligible.

Specific grinding energy: $$e_c = e_{ch} + e_{fr} + e_{def} + e_{kin} \quad (13)$$

In grinding, it is assumed that there is a minimum chip forming energy, which the grinding energy approximates for large chip thicknesses and material removal rates [17]. For large chip thicknesses, the friction and deformation energies, e_{fr} and e_{def}, decrease and chip formation becomes more effective [17].

The chip formation energy e_{ch} is dominated by shearing energy. Malkin and Joseph state that the specific shearing energy for chip formation during grinding is close to the specific melting energy of the material [17, 28]. This reasoning however is not intuitive because the material removal in grinding is based on shearing processes and the rim zone temperatures are lower than the melting temperature of the materials [11]. However, Malkin explains that the shear energy during chip formation approaches the melting energy limit, but since the shear resistance of the material decreases as the melting energy is approached, it seems unlikely that melting actually occurs [17].

Rasim et al. [29] were able to measure the forces during single grit scratch tests with a high-frequency force sensor. These tests simplify the grinding process by utilizing only a single grain in penetration with workpiece material [30, 31]. The energy per instantaneous scratch area either decreased or stayed constant over the scratch length which indicates that different energy sources dominate along the scratch path. In sum, the scratch test allows to measure the force to cause a single chip to form.

Equation 13 is usually used for the complete grinding process and incorporates all grit engagements. However, there can be many grits that do not cut but contribute to energy use through friction and plowing depending on wheel topography condition and kinematic parameters. In addition, the specific energy is not useful when the removed material volume approximates zero, as in polishing operations. Although a process with very little material removal transforms energy into frictional energy, the specific energy approximates infinity because per definition the energy is divided by a very small number.

Energy use also should be a function of cutting conditions, e.g. the temperature affects the friction, deformation and shearing energy. Furthermore, the chip geometry can vary widely for different grinding operations. As example, **Figure 1** shows how chip length and undeformed chip thickness from equations 1 and 2 vary for different grinding processes. Therefore, this study proposes to distinguish between the different engagement conditions of individual grits to understand the total energy consumption.

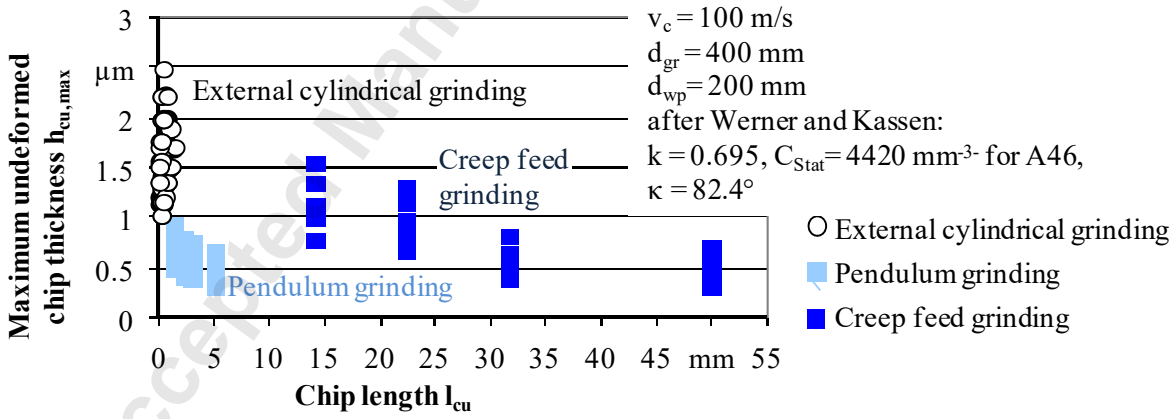

Figure 1 Chip length and undeformed chip thickness for different grinding kinematics with example parameters

ENERGY MODELLING

A new grinding energy model for ductile machining is proposed that incorporates grit size and chip thickness variation. It is hypothesized that a distributed grit model has higher prediction accuracy for process forces, energy, and surface roughness than a single chip thickness model. First, the chip thickness and length for an individual grit is deduced for a purely geometric penetration. Depending on the penetration depth, three phases of chip formation, elastic deformation (zone I), elastic and plastic deformation (zone II), and elastic and plastic deformation and chip formation (zone III), occur (**Figure 2**). In Figure 2 right, h_{cu} describes the chip thickness (excluding plowed and deformed material), whereas a_{e_grit} describes the actual grit engagement depth, which is larger than the chip thickness and includes elastically and plastically deformed material. In the following, friction, plowing, and shearing energies are discussed individually and then combined.

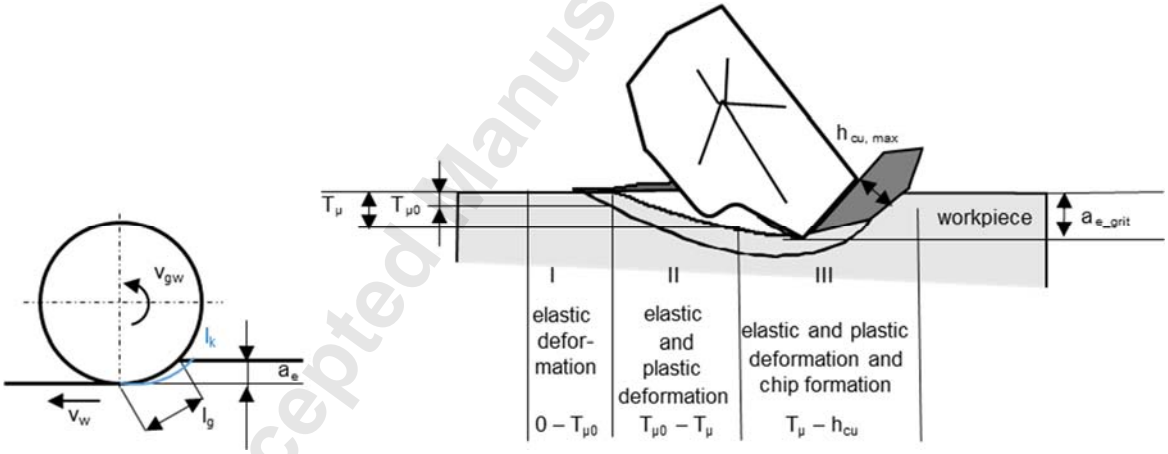

Figure 2 Left: Wheel engagement in surface grinding, Right: Grit engagement zones (after [4, 12])

Geometric chip thickness and length model

The following chip geometry model is developed here to incorporate the grinding process parameters, and calculates the theoretical maximum chip thickness and kinematic chip length from the grit engagement kinematics. The model excludes material elasticity and deformation. In addition, the model assumes that one grit cuts through the workpiece material after the prior grit. Only grinding with the tool circumference with transverse feed is considered. In the following, the grit distances from the wheel center point are equal to the wheel radius R.

Two grits on the grinding wheel are defined with time-dependent positions $\mathbf{x_1(t)}$ and $\mathbf{x_2(t)}$, defined as vectors (Figure 3). The case of a flat workpiece is assumed, but external and internal cylindrical grinding can easily be considered with using the equivalent wheel diameter from equation 3. This results in equations (14) and (15).

$$\begin{aligned}\boldsymbol{x}_1(t) &= \begin{pmatrix} x_1(t) \\ y_1(t) \end{pmatrix} = \begin{pmatrix} v_x \cdot t + R \cdot \sin(\omega \cdot t + \varphi_1) \\ v_y \cdot t + R \cdot (1 - \cos(\omega \cdot t + \varphi_1)) \end{pmatrix} \Rightarrow \\ \dot{\boldsymbol{x}}_1(t) &= \begin{pmatrix} \dot{x}_1(t) \\ \dot{y}_1(t) \end{pmatrix} = \begin{pmatrix} v_x + R \cdot \omega \cdot \cos(\omega \cdot t + \varphi_1) \\ v_y + R \cdot \omega \cdot \sin(\omega \cdot t + \varphi_1) \end{pmatrix}\end{aligned} \tag{14}$$

$$\begin{aligned}\boldsymbol{x}_2(t) &= \begin{pmatrix} x_2(t) \\ y_2(t) \end{pmatrix} = \begin{pmatrix} v_x \cdot t + R \cdot \sin(\omega \cdot t + \varphi_2) \\ v_y \cdot t + R \cdot (1 - \cos(\omega \cdot t + \varphi_2)) \end{pmatrix} \Rightarrow \\ \dot{\boldsymbol{x}}_2(t) &= \begin{pmatrix} \dot{x}_2(t) \\ \dot{y}_2(t) \end{pmatrix} = \begin{pmatrix} v_x + R \cdot \omega \cdot \cos(\omega \cdot t + \varphi_2) \\ v_y + R \cdot \omega \cdot \sin(\omega \cdot t + \varphi_2) \end{pmatrix}\end{aligned} \tag{15}$$

Where v_x is grinding wheel speed in x-direction, v_y is grinding wheel speed in y-direction, R is the wheel radius, φ_1 is the angle of grit 1, φ_2 is the angle of grit 2, t is time, and ω is wheel angular speed.

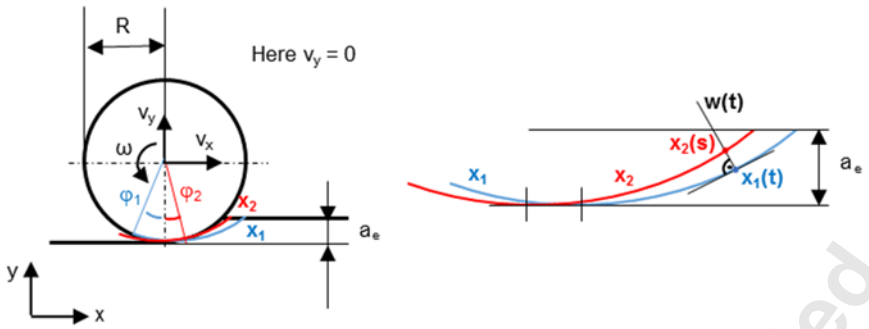

Figure 3 Grit trajectories

The direction of the chip thickness vector, $\mathbf{w_1}(t)$, is defined as being perpendicular to the tangent of speed $\dot{\boldsymbol{x}}_1(t)$ of grit 1 at the position, $\mathbf{x_1}(t)$ (equation 16). The vector length of the chip thickness vector, $\mathbf{w_1}(t)$, has to be found from its intersection with the position of the second grit, $\mathbf{x_2}(s)$, at another time s (equation 17). The time is different for both paths, so time s is used instead for path two $\mathbf{x_2}(t = s)$. The following conditions are required as described in equations (16-18).

$$\boldsymbol{w}_1(t)^T \cdot \dot{\boldsymbol{x}}_1(t) = 0 \tag{16}$$

$$\boldsymbol{x}_1(t) + r \cdot \boldsymbol{w}_1(t) = \boldsymbol{x}_2(s) \tag{17}$$

$$\boldsymbol{w}_1(t) = \begin{pmatrix} -\dot{y}_1(t) \\ \dot{x}_1(t) \end{pmatrix} \tag{18},$$

With $\dot{x}_1(t)$ is the velocity of grit one in x-direction and $\dot{y}_1(t)$ is the velocity of grit one in y-direction.

This leads to the following non-linear equation (19).

$$\underbrace{\begin{pmatrix} v_x \cdot t + R \cdot \sin(\omega \cdot t + \varphi_1) \\ v_y \cdot t + R \cdot (1 - \cos(\omega \cdot t + \varphi_1)) \end{pmatrix}}_{\boldsymbol{x}_1(t)} + r \cdot \underbrace{\begin{pmatrix} -v_y - R \cdot \omega \cdot \sin(\omega \cdot t + \varphi_1) \\ v_x + R \cdot \omega \cdot \cos(\omega \cdot t + \varphi_1) \end{pmatrix}}_{\boldsymbol{w}_1(t)}$$
$$= s \cdot \underbrace{\begin{pmatrix} v_x \\ v_y \end{pmatrix}}_{\boldsymbol{v}} + \underbrace{\begin{pmatrix} R \cdot \sin(\omega \cdot s + \varphi_2) \\ R \cdot (1 - \cos(\omega \cdot s + \varphi_2)) \end{pmatrix}}_{\boldsymbol{x}(s)} \quad (19)$$

There is no analytic solution, but the solution can be found iteratively. With the Gauss–Newton algorithm, the last vector is expanded by an appropriate start condition for the time s as follows in equation (20).

$$s = t + \frac{\varphi_1 - \varphi_2}{\omega} \quad (20)$$

Then follow equations 21 to 23 to find the chip thickness vector, $\mathbf{w_1}(t)$. The maximum length of $\mathbf{w_1}(t)$ is the undeformed maximum chip thickness, $h_{cu,max}$.

$$\boldsymbol{x}_1(t) + r \cdot \boldsymbol{w}_1(t) \approx \underbrace{(s + ds)}_{\hat{s}} \cdot \boldsymbol{v} + \underbrace{\begin{pmatrix} R \cdot \sin(\omega \cdot s + \varphi_2) \\ R \cdot (1 - \cos(\omega \cdot s + \varphi_2)) \end{pmatrix} + \underbrace{\begin{pmatrix} R \cdot \omega \cdot \cos(\omega \cdot s + \varphi_2) \\ R \cdot \omega \cdot \sin(\omega \cdot s + \varphi_2) \end{pmatrix}}_{\partial \boldsymbol{x}/\partial s} \cdot \underbrace{(\hat{s} - s)}_{ds}}_{\boldsymbol{x}_t(\hat{s})} \quad (21)$$

$$\boldsymbol{x}_1(t) + r \cdot \boldsymbol{w}_1(t) \approx s \cdot \boldsymbol{v} + ds \cdot \boldsymbol{v} + \underbrace{\begin{pmatrix} R \cdot \sin(\omega \cdot t + \varphi_1) \\ R \cdot (1 - \cos(\omega \cdot t + \varphi_1)) \end{pmatrix} + \begin{pmatrix} R \cdot \omega \cdot \cos(\omega \cdot t + \varphi_1) \\ R \cdot \omega \cdot \sin(\omega \cdot t + \varphi_1) \end{pmatrix} \cdot ds}_{\boldsymbol{x}_t}$$
$$\underbrace{\begin{pmatrix} \boldsymbol{w}_1(t) & -\boldsymbol{v} - \begin{pmatrix} R \cdot \omega \cdot \cos(\omega \cdot t + \varphi_1) \\ R \cdot \omega \cdot \sin(\omega \cdot t + \varphi_1) \end{pmatrix} \end{pmatrix}}_{\boldsymbol{A}} \cdot \begin{pmatrix} r \\ ds \end{pmatrix} = \underbrace{\begin{pmatrix} R \cdot \sin(\omega \cdot t + \varphi_1) \\ R \cdot (1 - \cos(\omega \cdot t + \varphi_1)) \end{pmatrix} + s \cdot \boldsymbol{v} - \boldsymbol{x}_1(t)}_{\boldsymbol{B}} \quad (22)$$

$$\Rightarrow \boldsymbol{A} \cdot \begin{pmatrix} r \\ ds \end{pmatrix} = \boldsymbol{B} \Leftrightarrow \begin{pmatrix} r \\ ds \end{pmatrix} = \boldsymbol{A}^{-1} \cdot \boldsymbol{B} \tag{23}$$

Critical penetration depths

It is traditionally assumed that chip formation starts when a critical depth of cut (or grain cutting depth), T_μ is reached [4, 32]. This critical shearing DOC (depth of cut) depends on cutting speed, material properties, and friction conditions, e.g. the cooling lubrication conditions. As cutting speed increases the critical shearing DOC decreases [32]. Rasim et al. [33] found correlations between the critical shearing DOC with the grit shape, in particular opening angle in cutting direction and apex angle. However, there are very few exact values available in the literature. Lortz [32] defined the critical shearing DOC at the depth when the cross-section of the groove is larger than the area of the side bulges (**Figure 4**); furthermore, Lortz assessed critical shearing depth of cut experimentally from tactile profile measurements (Table 1). The values for the critical shearing DOC in Table 1 unfortunately are much larger than many of the values for the average maximum undeformed chip thickness in **Figure 1**.

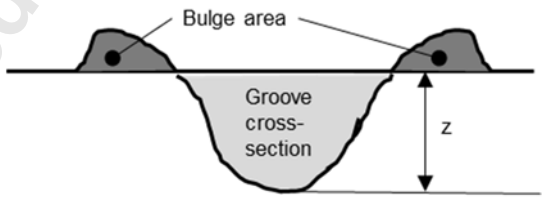

Figure 4 Groove cross-section and bulges from plowing

Table 1: Critical shearing depth of cut for different cutting speeds with a confidence level of 95%, values approximated from a diagram in [32]

Grinding wheel specification	EK601 6 Ke (corundum #60)
Grinding wheel diameter	d = 250 mm
Workpiece speed	v_w = 1 m/s
Workpiece material	steel Ck45N (0.45% C)
Coolant	None

Cutting speed [m/s]	Critical shearing depth of cut T_μ [µm]		
	Minimum	Average	Maximum
18	1.4	1.8	2.25
35	0.9	1.2	1.5
54	0.6	0.9	1.2

In addition to the critical shearing depth of cut, T_μ, it is proposed here to regard a critical plowing depth of cut, $T_{\mu 0}$, to distinguish between the zone I of elastic deformation and zone II of elastic and plastic deformation (**Figure 2**). Malkin and Guo discuss that plowing is controlled either by a critical depth or a critical rake angle of the cutting edge [17]. Only the critical-depth-controlled plowing can be accounted for the size effect that the energy per volume removed decreases with increasing chip thickness [17]. Three cases of cutting edge-workpiece

interaction are then possible for a single grain shape and depend on the maximum grit depth of cut, a_{e_grit} (**Figure 5**):

1. Cutting edge rubs against the workpiece (elastic deformation only, from depth 0 to $T_{\mu 0}$)

2. Cutting edge plows through the workpiece (elastic deformation + plastic deformation, from depth $T_{\mu 0}$ to T_{μ})

3. Cutting edge forms chip (elastic deformation + plastic deformation + chip formation by shearing, from T_{μ} to a_{e_grit})

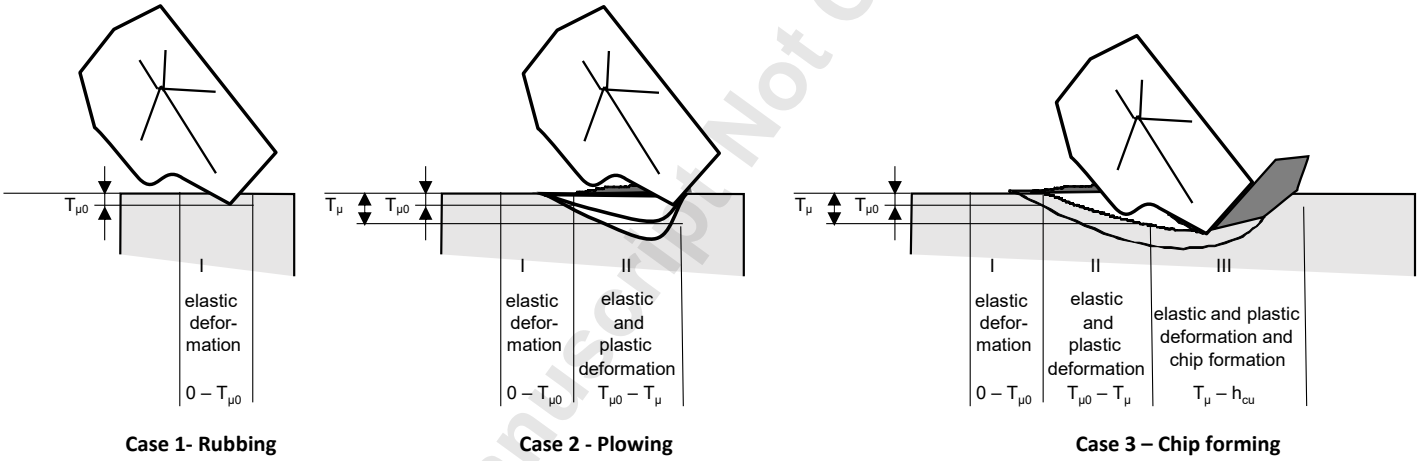

Figure 5 Three engagement cases depending on maximum grit depth of cut

In the following, a simplified distributed grit model is proposed which can differentiate between different engagement depths per grit. Equation (24) incorporates energies depending on engagement depth a_{e_grit}, critical shearing depth of cut T_{μ}, critical plowing depth of cut $T_{\mu 0}$. It is assumed that the total energy is a sum of individual grit energies.

For now, the critical depths T_μ and $T_{\mu 0}$ are assumed to be independent of the grit size and shape and friction conditions are constant. This simplified model can be used for tools with a narrow grit size and grit protrusion, for example applicable for engineering single-layer grinding wheels. In the following, the elastic and plastic deformation beneath the grit and kinetic chip energy are neglected.

$$E = \int_{t(y=0)}^{t(y=a_{e\_grit})} E_{fr}(t) + \int_{t(y=T_{\mu 0})}^{t(y=a_{e\_grit})} E_{pl}(t) + \int_{t(y=T_{\mu})}^{t(y=a_{e\_grit})} E_{ch}(t) \quad (24)$$

In the future, the model can be improved by incorporating more grit shape properties, grit tip angles, grit protrusion heights, and other factors, and expanding it to the whole grinding tool. For example, Jiang et al. [34] used a single grit force model to estimate the total grinding force in a toric grinding wheel.

Experimentally, energy and material conversion for all three cases can be studied by single grit scratch tests. Experimental findings in single grit scratch tests can also be compared with FEM simulations to further understanding of chip formation [35]. The following models for the three energies are based on analytical models and literature studies.

Friction energy model

In the following, rubbing and friction energy are used as synonyms. Hahn [9] hypothesized that rubbing forces on the clearance face of the abrasive grit play a major role compared to the cutting forces. Singh et al. [30] calculated a primary friction energy from the ratio of average power requirement to material removal rate. Singh et al. [30] utilized a

secondary friction energy from the abrasive grit and the workpiece material along the cutting edge over the total cutting path.

Wear flats, i.e. dulled flattened tips of the abrasive grains, increase the sliding energy [17]. Wear flats are generated by dressing, attritious wear, or adhesion of metal chips during grinding [17, 36]. Malkin and Cook found a correlation between tangential grinding force, F_t, and normal grinding force, F_n, with the wear flat area, A_a (equations 25 and 26) [17, 36].

Tangential grinding force: $F_t = F_{t,c} + \mu \bar{p} A_a$ (25)

Normal grinding force: $F_n = F_{n,c} + \bar{p} A_a$ (26)

Where $F_{t,c}$ is the tangential force for cutting, $F_{n,c}$ is the normal force for cutting, $\bar{p}$ is the average contact press, and μ is the friction coefficient

In the following, friction energy is calculated as the product of grit engagement length and normal grinding force per grit (equation 27).

Friction energy: $E_{fr} = \int_{t(y=0)}^{t(y=a_{e\_grit})} F_{n,grit} \cdot l_k(t) dt$ (27)

For the specific normal grinding force per grit, Werner assumed a function of the local chip cross-sectional area and the local number of kinematic cutting edges (equation 28) [15].

Specific normal force per grit: $F'_n = \int_0^{l_k} k \, (\bar{Q}(l))^n \cdot N_{dyn}(l) \cdot dl$ (28)

Where $\bar{Q}(l)$ is the local chip cross-section, k is the factor between force and cutting area, and is material dependent. Werner found factor k to be equal to 80 kp/mm^2 for his experiments with low-carbon steel (C45) [15]. Factor k is in similar magnitude of the material strength.

For this study, we assume the normal force per grit to be the total normal force F_n (which can be measured with a force sensor) divided by the number of cutting edges per area, C_{stat} (equation 29).

Total normal force per grit: $F_{n,grit} = \frac{F_n}{C_{stat}}$ (29)

Plowing energy model

The specific plowing energy is often approximated as being equal to the indentation hardness of the material being plowed, which implies that the geometry of the plowed groove would have no effect on the specific plowing energy [37, 38]. Singh et al. [30] calculated the specific plowing energy from scratch hardness and indentation hardness. However, the geometry of the grooves in grinding depends on the grit shape (**Figure 6**).

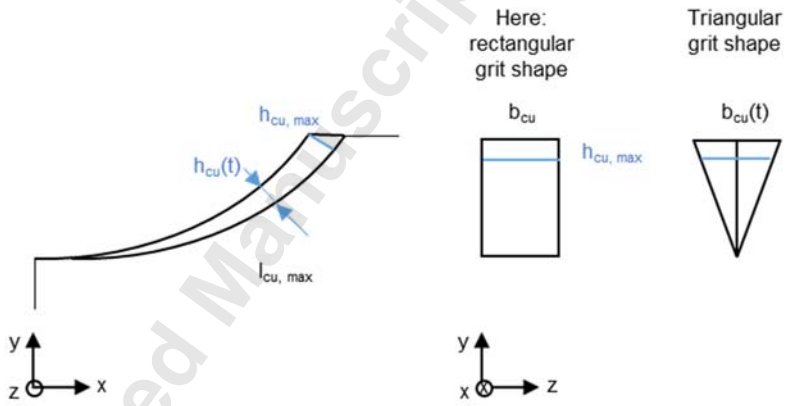

Figure 6 Chip geometry according to [11, 17] with grit width b_{cu}

Shaw [11, 39] approximated the specific energy from a spherical grain model as follows in equation (30). This equation includes indentation energy and surface shearing energy. The ratio t/d_g is a measure of grain sharpness.

Specific spherical grit cutting energy: $e_c = \frac{3\pi}{4} \cdot \frac{H}{\beta} \cdot \frac{C\prime}{3} \cdot \left(2 + \mu \sqrt{\frac{d_g}{t_{indent}}}\right)$ (30)

With H is the workpiece hardness, β is the upward flow ratio, C' is the constraint coefficient, μ is friction coefficient, d_g is grain diameter, and t_{indent} is the indentation depth

In equation (31), for a rectangular grit the plowing energy is calculated from the area of displacement multiplied by material hardness. The area is viewed in grit movement direction only and calculated as the grit tip width in z-direction b_{cu} multiplied with the chip thickness h_{cu}. The grit engagement length is considered through the engagement time from grit depth $T_{\mu 0}$ until a_{e_grit}.

Plowing energy: $E_{pl} = \int_{t(y=T_{\mu 0})}^{t(y=a_{e\_grit})} b_{cu}(t) \cdot h_{cu}(t) \cdot l_k(t) \cdot H \, dt$ (31)

Shearing energy model

Force and shearing analysis in machining has a long history. The work of Merchant [40] on force circles during orthogonal cutting is still valid and much cited to explain shearing processes in cutting and grinding. In Werner's studies, the shearing force made up only 3% of the total cutting force [15].

With analogy to chipless shearing process such as blanking or punching, the shearing force will be calculated from material shear strength S and cross-sectional area A_{shear}, which is sheared (**Figure 7**) [41].

Shearing force: $F_{shear} = S \cdot A_{shear}$ (32)

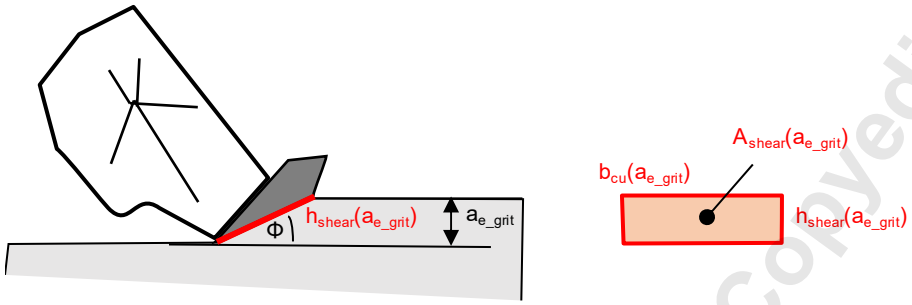

Figure 7 Shearing area

Shear strength is usually assumed from the ultimate tensile strength. For example, for alloy steel shear strength is 75% of ultimate tensile strength (S = 0.75% * 500...740 MPa = 375…555 MPa for X10CrNi18-8). For the calculations here, shear area A_{shear} comes from the grit tip width b_{cu} and shear height h_{shear} (equation 33, **Figure 7**). Shear height is a function of chip thickness and shear angle ϕ (equation 34). The shear plane is located at the point of the maximum shear stress its angle [27]. In orthogonal cutting, the shear angle can be from the rake angle and friction angle [27, 40]. The tangent of the friction angle is the friction coefficient between sliding chip and tool face [40], which depends on lubrication conditions and temperature. Therefore, finding the shear angle is not trivial and depends on process conditions. Minimum shear energy is at a shear angle of about 45° [11, 42].

Shear area: $A_{shear} = b_{cu} \cdot h_{shear}$ (33)

Shear height: $h_{shear} = \frac{h_{cu}(t)}{sin\phi}$ (34)

Then, shearing energy is equal to shear force over shear length.

Shearing Energy: $E_{ch} = \int_{t(y=T_\mu)}^{t(y=a_{e\_grit})} F_{shear} \cdot l_k(t)dt$ (35)

MODELING RESULTS AND DISCUSSION

The selected equations for friction, plowing, and shearing energy are integrated to calculate the total energy (**Figure 8**). In the following, no variation of grit shape, angle, protrusion height, or distance between grits is considered. Each grit has only one cutting edge. The grits are assumed to be blocks with a width b_{cu} in z-direction. The angular difference between the grit engagements is calculated using the grinding wheel diameter, d_{eq}, and areal cutting edge density, C_{stat}. Equation (36) is then used to calculate the angle difference between two cutting edges.

Angular cutting edge distance: $\varphi_2 - \varphi_1 = \frac{2\pi}{Cutting\ edge\ number\ on\ circumference} = \frac{2\pi}{2\pi \cdot \frac{d_{eq}}{2}\sqrt{C_{stat}}}$.

(36)

At this time, all energies and forces are simply added to the total energy and force respectively; but in the future coupling effects can be implemented, for example how temperature rise from friction impacts shear strength and shearing. To achieve this, the variables could be modeled as being time-dependent. A simulation was run utilizing equation 24 and the model developed in previous sections to calculate the formation geometry of the chip, the total forces per chip, and the specific total processing-energy per chip, excluding

machine and background energy. The specific energy is the energy divided by the chip volume, including undeformed chip thickness, grit width and chip length (equation 37).

$$\text{Chip volume} = \int_{t(y=0)}^{(y=a_{e_{grit}})} b_{cu}(t) \cdot h_{cu}(t) \cdot l_k(t) dt \qquad (37)$$

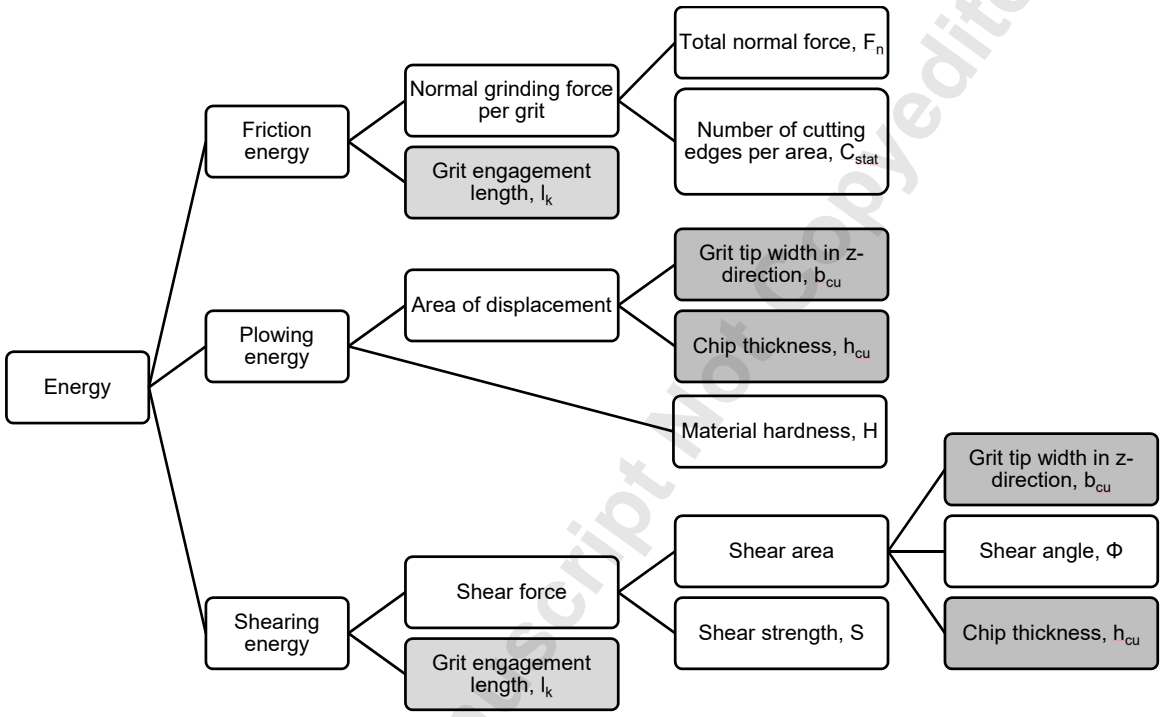

Figure 8 Energy model overview; shaded boxes show reoccurring chip geometry values.

The simulation was run for 3 equidistant grits (with one cutting edge per grit only) engaging with the workpiece under several parameters (Table 2). Six simulation runs are reported here (A-F) which vary six of the input parameters; these include machine tool control parameters (speed, feed, and depth of cut), and workpiece-process interaction parameters (engaged cutting edges and critical depth of cut). Simulation run A is a baseline used for comparison against runs B-F.

Table 2 Simulation parameters and results

Settings			**A**	**B**	**C**	**D**	**E**	**F**
Wheel circumf. speed	v_{gr}	m/s	35	**70**	**70**	35	35	35
Feed rate in x-dir.	$v_x = v_w$	m/min	60	60	**120**	60	60	60
Depth of cut	a_e	mm	0.5	0.5	0.5	**1**	0.5	0.5
Equiv. wheel diameter	d_{eq}	mm	250	250	250	250	250	250
Grinding wheel width	b_{gr}	mm	10	10	10	10	10	10
Grit tip width in z-dir.	b_{cu}	mm	0.01	0.01	0.01	0.01	0.01	0.01
Av. no. of cutting edges	C_{stat}	$1/mm^2$	1	1	1	1	1	**2**
Critical plowing DOC	$T_{\mu 0}$	µm	0.25	0.25	0.25	0.25	**0.5**	0.25
Critical shearing DOC	T_{μ}	µm	0.75	0.75	0.75	0.75	**1.5**	0.75
Shear angle	ϕ	°	45	45	45	45	45	45
Specific normal force	F'_n	N/mm	10	10	10	10	10	10
Hardness	H	N/mm^2	1700	1700	1700	1700	1700	1700
Shear strength	S	N/mm^2	400	400	400	400	400	400
Maximum chip length	l_{k_max}	**mm**	**10.4747**	**10.3294**	**10.4747**	**15.2444**	**10.4747**	**10.7759**
Max. undef. chip thickness	$h_{cu,\ max}$	**µm**	**1.2419**	**0.62969**	**1.2419**	**1.7558**	**1.2419**	**0.87817**
Theor. chip volume		**μm^3**	**118470**	**59233**	**118470**	**250780**	**118470**	**88653**
Number of cutting edges in the contact area			**104.7**	**103.3**	**104.7**	**152.4**	**104.7**	**215.5**
Friction force		**µN**	**82.943**	**85.29**	**82.943**	**80.526**	**82.943**	**40.312**
Plowing force		**µN**	**42.199**	**21.396**	**42.199**	**59.625**	**42.199**	**29.839**
Shearing force		**µN**	**14.042**	**7.1195**	**14.042**	**19.841**	**14.042**	**9.9292**
Specific friction energy per chip		**J/mm^3**	**3.3414**	**6.7768**	**3.3414**	**2.2959**	**3.3414**	**2.2967**
Specific plowing energy per chip		**J/mm^3**	**2.0292**	**1.9693**	**2.0293**	**1.927**	**1.967**	**1.8978**
Specific shearing energy per chip		**J/mm^3**	**0.61998**	**0.44021**	**0.61999**	**0.61512**	**0.43334**	**0.52706**
Specific total energy per chip		**J/mm^3**	**5.99058**	**9.18631**	**5.99069**	**4.83802**	**5.74174**	**4.72156**

The friction, plowing and shearing forces sum to the total force. All forces are time-dependent and can be displayed as shown in **Figure 9**. The three zones depend on the critical shearing DOC and critical plowing DOC which can be seen as jumps in the forces. Rasim et al. reported maximum forces of about 30 N in normal direction and about 12 N in tangential direction in single grit scratch tests with CBN grits (B213) on high-carbon steel (100Cr6) with DOC of 0.75 mm and grinding wheel speed of 10 m/s [29]. Singh et al. measured normal plowing forces in single grit scratch tests on mild steel of 3.39 – 9.61 N [30]. Wang et al. measured normal forces of up to 20 N for scratch annealed pure titanium [43]. The much higher forces in single grit scratch tests compared to the ones simulated here can be explained by higher loads in the experiments because a single grit performs the complete cut whereas a grit experiences lower loads in the simulation because one grit cuts what is left over from the previous grit in the simulation; i.e. the simulation grit cuts in a trough, following the path of a prior grit.

The resulting energies are displayed in **Figure 10**. The specific energies are the maximum energy divided by the total theoretical chip volume. Specific energies for the whole tool range from 2.5 – 82 J/mm^3 for metal grinding (aluminum, cast iron, and steel) [44]. Malkin and Guo specified a minimum value of 13.8 J/mm^3 for grinding high-carbon steel (AISI 1095) with alumina wheels, which is also the specific shearing force energy [17]. Singh et al. measured specific plowing energies for single grit scratch tests of 8.65 – 37.1 J/mm3 for mild steel [30].

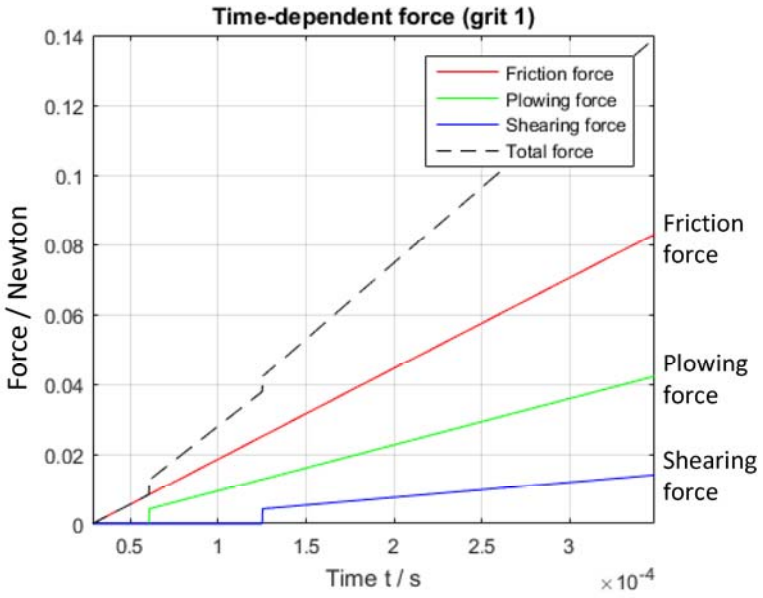

Max. friction force	0.082943 N
Max. plowing force	0.042199 N
Max. shearing force	0.014042 N

Figure 9 Forces for the engagement of one cutting edge, setting A from Table 2

If the wheel circumferential speed is doubled (setting B, Table 2), but all other parameters including feed speed and normal force stay constant, the chip thickness is reduced by about 50%, as are the plowing and shearing forces which depend on the chip thickness. The chip volume change is decreased to half as well, so the specific friction energy per chip is doubled. Specific plowing energy almost remains the same whereas the specific shearing energy is reduced to 71%.

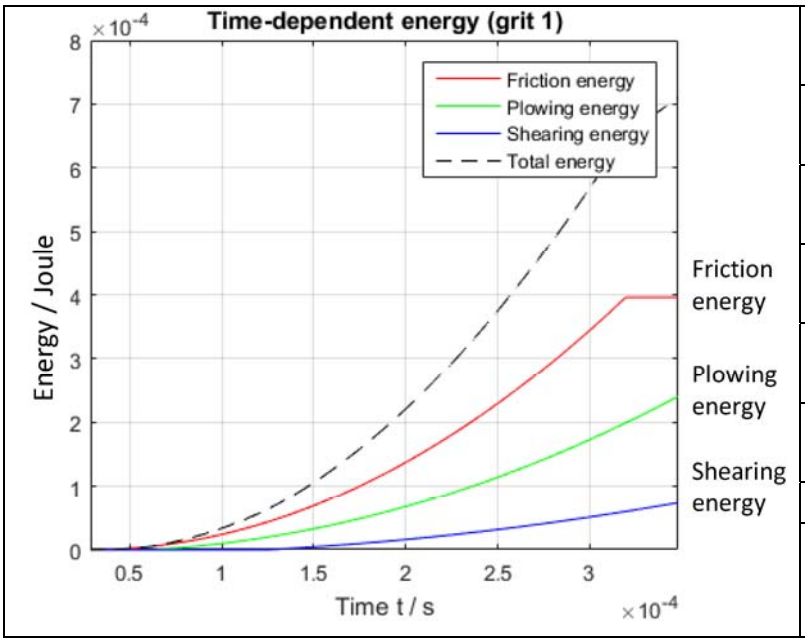

Max. friction energy	0.00039584 J
Specific friction energy	3.3414 J/mm^3
Max. plowing energy	0.0002404 J
Specific plowing energy	2.0292 J/mm^3
Max. shearing Energy	0.000073447 J
Specific shearing energy	0.61998 J/mm^3
Total energy	0.000709687 J
Specific total energy	5.99058 J/mm^3

Figure 10 Energies for the engagement of one cutting edge, setting A from Table 2

If the feed rate is increased so that the speed ratio between wheel circumferential speed and feed rate remains constant (setting C, Table 2), all results from setting A and C are the same. However, in reality the normal force F_n would change. Doubling the depth of cut (from setting A to setting D, Table 2), results in 145% and 141% larger chip length and chip thickness respectively. The theoretical chip volume increases to 212%. The friction force remains almost constant, whereas plowing and shearing forces both rise to 141%. The specific total energy decreases to 80%. This comes from increased chip length and increased number of active grits with higher cutting depth (Table 2).

If the critical plowing depth of cut and critical shearing depth of cut are each doubled (from setting A to setting E, Table 2), only the plowing and shearing energies are affected. The total and specific plowing and shearing energies are decreasing to 96.9% and 69.9%

respectively, because the respective zones start later. Increasing the cutting edge number by 100% (from setting A to setting F, Table 2) results in a lower specific total energy of 79%.

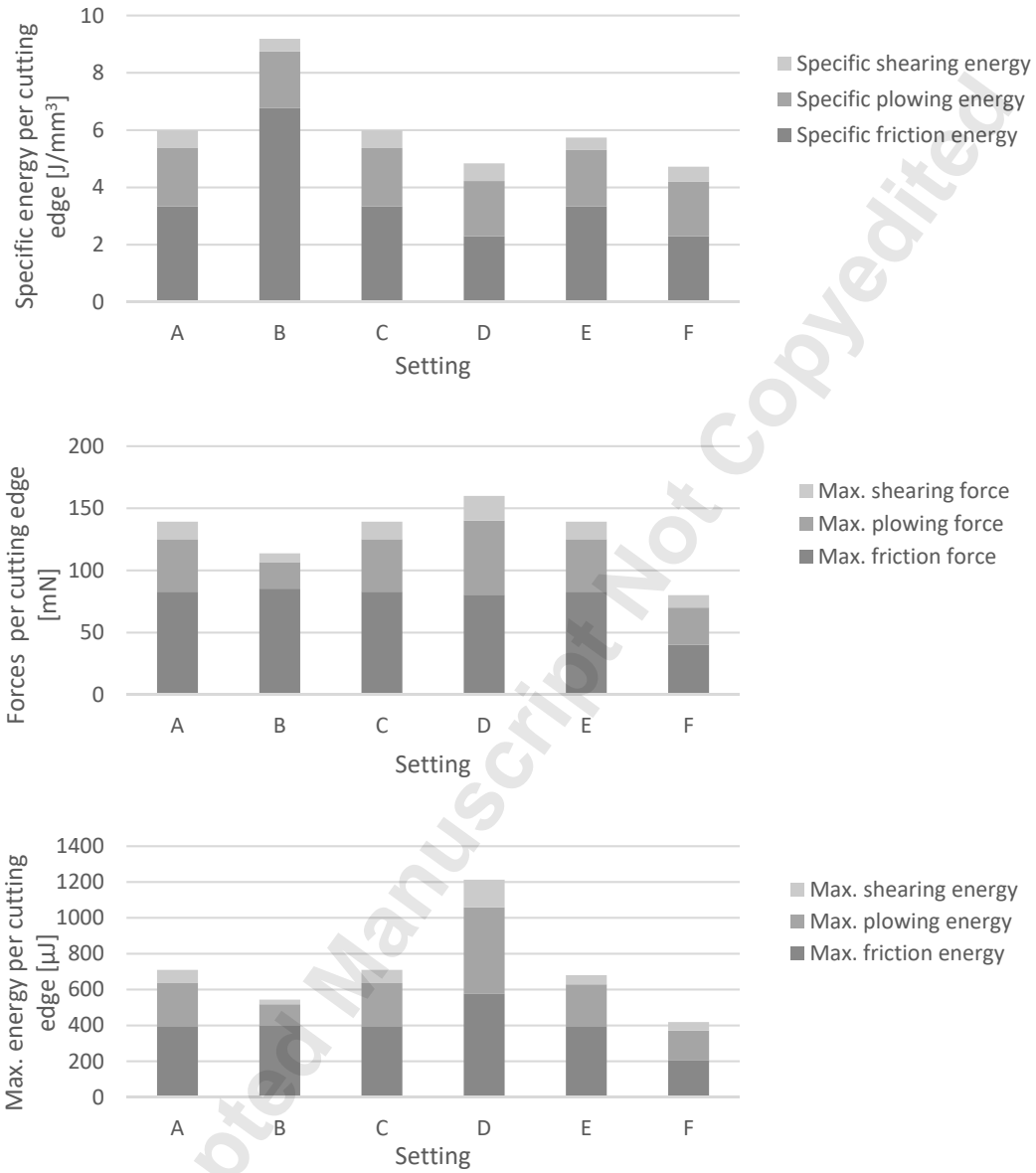

Figure 11 Comparison of the six settings with respect to specific energy, forces and maximum energy per cutting edge

All settings can be compared with regard to their specific energies, forces and maximum energies per cutting edge are compared (**Figure 11**). Specific and maximum friction energy is

always the largest part of the specific or maximum energy, followed by plowing and shearing energy. The friction force is calculated from the normal force and number of cutting edges (equation 29) and therefore constant for settings A – E with constant cutting edge density. Specific energy per cutting edge is lowest for setting D where the depth of cut is larger and therefore a larger chip volume is achieved. Energies and forces are lowest for setting F where the cutting edge density is higher, so the load is distributed on more cutting edges.

CONCLUSION AND OUTLOOK

The individual energy models are comparable with models in the literature. They include chip length and can therefore apply to different process kinematics, such as external cylindrical, surface creep feed and pendulum grinding with their distinct chip geometries. However, the grinding energy model needs to be tested more analytically and compared with experimental data. Furthermore, the model needs to be refined with varying grit sizes, grit geometries, grit orientation, and grit protrusion to analyze the distribution of energies. Besides the grit properties, the energies for friction, plowing and cutting depend on the grit properties, such as size, orientation, protrusion, tip angle, as well as kinematic parameters - including bond elasticity and other properties - cooling lubricant conditions at the individual grit, and more. Furthermore, time-dependent variables and varying shear angles need to be considered.

In the future, the model can also be expanded on brittle materials, but crack propagation and particle break-out will replace the chip formation zones. Moreover, all forces can be modeled as coupled. For example, if the shear plane angle increases, the shearing

energy in the shear plane decreases, but the rubbing energy at the rake face increases [11]. For now, this was neglected in the discussed model.

Common specific energy models relate the total energy to volume removed. However, this results in unfavorably high numbers for specific energy for finishing operations because only small material volumes are removed. Introducing energy-based metrics with other denominators such as achieved surface quality can be more useful efficiency indicators [45].

ACKNOWLEDGMENT

Part of this research was funded by the German research foundation (DFG) within the IRTG 2057 “Physical Modeling for Virtual Manufacturing Systems and Processes”.

NOMENCLATURE

A_a	wear flat area
a_e	depth of cut
a_{e_grit}	maximum grit depth of cut
A_{shear}	shear area
b_{cu}	grit tip width (in z-direction)
b_{gr}	grinding wheel width
C'	constraint coefficient

C_{stat}	(static) areal cutting edge density, number of cutting edges per area
d_{eq}	equivalent grinding wheel diameter
d_g	grain diameter
d_{gr}	grinding wheel diameter
d_w	workpiece diameter
H	workpiece hardness
h_{cu}	chip thickness
$h_{cu,max}$	maximum undeformed chip thickness
h_{shear}	shear height
e_c	Specific grinding energy
e_{ch}	specific energy for forming of grinding chips
e_{def}	specific energy for deforming and plowing material
e_{fr}	specific energy for sliding and overcoming friction between grinding grits, tool bond, and workpiece
e_{kin}	specific kinetic energy of the chips
E	energy
E_{fr}	friction energy
E_{pl}	plowing energy

E_{ch}	cutting energy
F'_n	specific normal force
F_a	axial grinding force
F_n	normal grinding force
$F_{n,\,grit}$	normal force per grit
$F_{n,c}$	normal force for cutting
F_t	tangential grinding force
$F_{t,\,c}$	tangential force for cutting
F_{shear}	shearing force
K	factor between force and cutting area; material dependent; of similar magnitude to material strength
l_g	Static chip length
l_k	kinematic chip length
P_c	processing power, cutting power
q	speed ratio
q_t	total heat flux; a sum of the heat into chip, coolant, grinding wheel and workpiece
$\bar{Q}(l)$	local chip cross-section

Q_w	material removal rate
r	proportionality factor between chip width and thickness
R	wheel radius; grit distances from the wheel center point
S	shear strength
s	time for second grit
t_{indent}	indentation depth
t	time for first grit
T_μ	critical shearing depth of cut
$T_{\mu 0}$	critical plowing depth of cut
v_c	cutting speed
v_{fr}	radial feed rate
v_{fa}	axial feed rate
v_{gr}	grinding wheel speed
v_w	workpiece speed
v_x	grinding wheel speed in x-direction
v_y	grinding wheel speed in y-direction
$\boldsymbol{w_1(t)}$	perpendicular vector
x	Horizontal position

$\boldsymbol{x_1(t)}$	time dependent position vector of grit 1
$\boldsymbol{x_2(t)}$	time dependent position vector of grit 2
y	vertical position
β	upward flow ratio
μ	friction coefficient
φ_1	angle of grit 1
φ_2	angle of grit 2
ω	wheel angular speed

REFERENCES

1. Haapala, K.R., et al., *A Review of Engineering Research in Sustainable Manufacturing.* Journal of Manufacturing Science and Engineering, 2013. **135**(4): p. 041013-041013.
2. *U.S. Energy Information Administration*. AEO [consumption.cfm] 2013 April 19, 2013; Available from: http://www.eia.gov/forecasts/aeo/er/early.
3. Allen, D., et al., *Environmentally benign manufacturing: Trends in Europe, Japan and USA.* Journal of Manufacturing Science and Engineering, 2002. **124**: p. 908–920.
4. Klocke, F., *Manufacturing Processes 2 – Grinding, honing, lapping*. 2009: Springer.
5. Marinescu, I.D., Hitchiner, M., Uhlmann, E., Rowe, W.B., Inasaki, I., *Handbook of Machining with Grinding Wheels*. 2007: CRC Press.
6. Baniszewski, B., *An environmental impact analysis of grinding*. 2005, Massachusetts Institute of Technology.
7. Aurich, J., M. Carrella, and M. Steffes, *Evaluation of Abrasive Processes and Machines with Respect to Energy Efficiency*, in *Leveraging Technology for a Sustainable World*, D.A. Dornfeld and B.S. Linke, Editors. 2012, Springer Berlin Heidelberg. p. 329-333.
8. Ding, H., et al., *An investigation on quantitative analysis of energy consumption and carbon footprint in the grinding process.* Proceedings of the Institution of Mechanical Engineers, Part B: Journal of Engineering Manufacture, 2014. **228**(6): p. 950-956.
9. Hou, Z.B. and R. Komanduri, *On the mechanics of the grinding process – Part I. Stochastic nature of the grinding process.* International Journal of Machine Tools and Manufacture, 2003. **43**(15): p. 1579-1593.
10. Linke, B.S., *Review on Grinding Tool Wear With Regard to Sustainability.* Journal of Manufacturing Science and Engineering, 2015. **137**(6): p. 060801-060801-8.
11. Rowe, W.B., *Principles of modern grinding technology*. 2009: William Andrew.

12. Tönshoff, H.K., et al., *Modelling and Simulation of Grinding Processes.* CIRP Annals - Manufacturing Technology, 1992. **41**(2): p. 677-688.
13. Mladenovic, G., et al., *Experimental Investigation of Microcutting Mechanisms in Oxide Ceramic CM332 Grinding.* Journal of Manufacturing Science and Engineering, 2015. **137**(3): p. 034502-034502-5.
14. Bifano, T.G. and S.C. Fawcett, *Specific grinding energy as an in-process control variable for ductile-regime grinding.* Precision Engineering, 1991. **13**(4): p. 256-262.
15. Werner, G., *Kinematik und Mechanik des Schleifprozesses*. **1971**, RWTH Aachen University.
16. Kassen, G., *Beschreibung der elemantaren Kinematik des Schleifvorgangs*. 1969, RWTH Aachen University.
17. Malkin, S., Guo, C., *Grinding technology : theory and application of machining with abrasives*. Vol. 2nd edition. 2008: Industrial Press.
18. Jin, T. and D. Stephenson, *Three Dimensional Finite Element Simulation of Transient Heat Transfer in High Efficiency Deep Grinding.* Annals of the CIRP, 2004. **53/2/2004**: p. 259 – 262
19. D., S. and J. T. *Physical basics in grinding*. in *1st European Conference on Grinding*. 2003. Aachen: VDI Verlag.
20. Linke, B. and M. Overcash, *Life Cycle Analysis of Grinding*, in *Leveraging Technology for a Sustainable World*, D.A. Dornfeld and B.S. Linke, Editors. 2012, Springer Berlin Heidelberg. p. 293–298.
21. Dahmus, J.B. and T.G. Gutowski. *An Environmental Analysis of Machining*. in *Proceedings 2004 ASME International Mechanical Engineering Congress and RD&D Expo*. 2004. Anaheim, California USA.
22. Gutowski, T., J. Dahmus, and A. Thiriez. *Electrical Energy Requirements for Manufacturing Processes*. in *Proceedings of the 13th CIRP International Conference on LCE*. 2006. Leuven, Belgium.
23. Chen, X., et al., *A Grinding Power Model for Selection of Dressing and Grinding Conditions.* Journal of Manufacturing Science and Engineering, 1999. **121**(November): p. 632-637.
24. Shaw, M.C., *Energy Conversion in Cutting and Grinding*.* CIRP Annals - Manufacturing Technology, 1996. **45**(1): p. 101-104.
25. Zein, A., et al. *Energy Efficiency Measures for the Design and Operation of Machine Tools: An Axiomatic Approach*. in *Proc. of the 18th CIRP Conf. on Life Cycle Engineering*. 2011. Braunschweig, Germany.
26. Hahn, R.S., *On the mechanics of the grinding process under plunge cut conditions.* Transactions of the ASME, Journal of Engineering for Industry, 1966: p. 72-80.
27. Tönshoff, H.K. and B. Denkena, *Basics of Cutting and Abrasive Processes*. Lecture Notes in Production Engineering. 2013.
28. Malkin, S. and N. Joseph, *Minimum energy in abrasive processes.* Wear 1975. **32 (1975)**: p. 15 – 23
29. Rasim, M., F. Klocke, and M. Weiß. *Identifikation der Spanbildungsphasen beim Schleifen*. in *3rd international Chemnitz manufacturing colloquium ICMC 2014*. 2014. Chemnitz, Germany.
30. Singh, V., P. Venkateswara Rao, and S. Ghosh, *Development of specific grinding energy model.* International Journal of Machine Tools and Manufacture, 2012. **60**: p. 1-13.
31. Li, X., et al., *The study on the influences of superabrasive grain spatial orientation for microcutting processes based on response surface methodology.* The International Journal of Advanced Manufacturing Technology, 2013. **67**(5): p. 1527-1536.
32. Lortz, W., *Schleifscheibentopographie und Spanbildungsmechanismus beim Schleifen*. 1975, RWTH Aachen University: Aachen.
33. Rasim, M., P. Mattfeld, and F. Klocke, *Analysis of the grain shape influence on the chip formation in grinding.* Journal of Materials Processing Technology, 2015. **226**: p. 60-68.

34. Jiang, Z., et al., *Predictive Modeling of Grinding Force Considering Wheel Deformation for Toric Fewer-Axis Grinding of Large Complex Optical Mirrors.* Journal of Manufacturing Science and Engineering, 2016. **138**(6): p. 061008-061008-10.
35. Rasim, M., F. Klocke, and P. Mattfeld, *Energy Model for Grinding Processes*, in *Thermo-energetic Design of Machine Tools*, K. Großmann, Editor. 2015, Springer International Publishing: Switzerland. p. 35-47.
36. Malkin, S. and N.H. Cook, *The wear of grinding wheels, Part 1 – Attritious wear.* Trans. of the ASME, 1971(Nov.): p. 11209-1128.
37. Hwang, T.W. and S. Malkin, *Upper bound analysis for specific energy in grinding of ceramics.* Wear, 1999. **231**(2): p. 161-171.
38. Rabinowicz, E., *Friction and Wear of Materials*. 2nd edition ed. 1995, New York: Wiley.
39. Shaw, M.C. *A new theory of grinding*. in *International Conference on Science in Industry, Monash University, Australia, 1-16.* 1971.
40. Merchant, E., *Mechanics of the metal-cutting process.* Journal of Applied Physics, 1945. **16**(207).
41. Kalla, D., J. Twomey, and M. Overcash, *MR2 Shearing Process - Unit Process Life Cycle Inventory* 2009.
42. Rowe, G.W., *Elements of metalworking theory*. 1979, London: Edward Arnold.
43. Wang, H., G. Subhash, and A. Chandra, *Characteristics of single-grit rotating scratch with a conical tool on pure titanium.* Wear, 2001. **249**(7): p. 566-581.
44. Kalpakjian, S. and S. Schmid, *Manufacturing Engineering and Technology*. 2010, New Jersey: Pearson Prentice Hall.
45. Linke, B., *Sustainability Indicators for Grinding Applied to Dressing Strategies.* Journal of Manufacturing Science and Engineering, 2013. **135**(5): p. 054502-054502.

Figure Captions List

Fig. 1 Chip length and undeformed chip thickness for different grinding kinematics with example parameters

Fig. 2 Left: Wheel engagement in surface grinding, Right: Grit engagement zones (after [4, 12])

Fig. 3 Grit trajectories

Fig. 4 Groove cross-section and bulges from plowing

Fig. 5 Three engagement cases depending on maximum grit depth of cut

Fig. 6 Chip geometry after [11, 17] with grit width b_{cu}

Fig. 7 Shearing area

Fig. 8 Energy model overview; shaded boxes shows reoccurring chip geometry values.

Fig. 9 Forces for the engagement of one cutting edge, setting A from Table 2

Fig. 10 Energies for the engagement of one cutting edge, setting A from Table 2

Fig. 11 Comparison of the six settings with respect to specific energy, forces and maximum energy per cutting edge

Table Caption List

Table 1 Critical shearing depth of cut for different cutting speeds with a confidence level of 95%, values approximated from a diagram in [32]

Table 2 Simulation parameters and results